Towards structural dynamics in condensed chemical systems exploiting ultrafast time-resolved x-ray absorption spectroscopy

Christian Bressler
Institut de Physique de la Matière Condensée, Université de Lausanne, CH-1015 Lausanne-Dorigny, Switzerland

Melanie Saes
Institut de Physique de la Matière Condensée, Université de Lausanne, CH-1015 Lausanne-Dorigny, Switzerland and Swiss Light Source, Paul Scherrer Institut, CH-5232 Villigen-PSI, Switzerland

Majed Chergui
Institut de Physique de la Matière Condensée, Université de Lausanne, CH-1015 Lausanne-Dorigny, Switzerland

Daniel Grolimund and Rafael Abela
Swiss Light Source, Paul Scherrer Institut, CH-5232 Villigen-PSI, Switzerland

Philip Pattison
Institut de Cristallographie, Université de Lausanne, CH-1015 Lausanne-Dorigny, Switzerland

(Received 22 August 2001; accepted 21 November 2001)

We present the case for exploiting time-resolved x-ray absorption to study structural dynamics in the liquid phase. With this aim in mind and considering the large differences between absorption coefficients in the optical and the x-ray domains as well as the x-ray absorption cross sections due to unexcited species, we have estimated the anticipated signal-to-noise ratio (S/N) under realistic conditions with femtosecond laser pump pulses and synchrotron radiation x-ray probe pulses. As a model system, we examine I^- photodetachment in water and detect the appearance of laser-generated neutral I atoms by their x-ray near-edge absorption structure (XANES) and by their extended x-ray absorption fine structure (EXAFS). While the S/N ratio critically depends on the photolysis yield, which itself is governed by the optical absorption cross section, the optimum sample concentration varies in a complex fashion as a function of pump laser intensity and optical absorption cross section. However, concentrations yielding near total absorption of the pump laser deliver quite optimum S/N ratios. The calculations presented here provide guidelines for the implementation of time-resolved x-ray absorption experiments in condensed phase chemical systems. © *2002 American Institute of Physics.* [DOI: 10.1063/1.1435618]

I. INTRODUCTION

Visualizing nuclear motion during a chemical reaction is crucial for our understanding of fundamental aspects of chemistry. With the advent of femtosecond spectroscopy this has become possible in *real time*, and a huge development took place in the 1990s, which culminated with the Nobel Prize for Chemistry in 1999.[1] The basic principle of femtosecond spectroscopy lies in the use of two optical ultrashort laser pulses: the first one (called the pump pulse) initiates a reaction via absorption of light by the system under study, while the second one follows the evolution of the system using spectroscopic observables.

Optical photons access valence electrons, which are usually distributed over multiple atoms. In general, structural information is derived via an *a priori* knowledge of the involved potential energy surfaces. This, along with molecular dynamics (MD) or wavepacket simulations, can provide the desired structural dynamical information, including snapshots of reaction intermediates.[1] With increasing complexity of the system under investigation, overlapping bands and unknown potential energy surfaces hamper this visualization of ongoing chemical reactions. Therefore, optical spectroscopy is not easy to translate into structure, except in a few rare cases. On the other hand, structural techniques, such as diffraction with electrons or x rays, or x-ray spectroscopy such as EXAFS (extended x-ray absorption fine structure), have proven to be powerful techniques for structural determination of many-body systems with a high spatial resolution. Inversion of the data to atomic coordinates is in addition straightforward. Therefore, one could, in principle, combine the direct inversion advantages of these techniques and their high spatial resolution with the high temporal resolution of ultrafast pump-probe techniques, provided sufficiently short duration electron or x-ray pulses can be generated.

The Zewail group pioneered the electron diffraction scheme,[2–5] with which they successfully monitored reaction intermediates in both CH_2I_2 and in $Fe(CO)_5$ dissociation processes using picosecond electron pulses. Most groups, however, have adopted x-rays. Rentzepis and co-workers[6–8] have used ultrafast laser-triggered diodes to produce x-ray pulses of $\leqslant$10 ps duration. With this technique, they studied laser-triggered melting in GaAs by time-resolved diffraction methods. In another approach, Wilson, Kieffer, and their co-

workers used ultra short duration (~1 ps and even less) bursts of x-radiation generated from laser-produced plasmas for structural dynamics studies.[9–12] The limitation of this x-ray source (as well as with laser-triggered x-ray diodes) lies in the isotropic emission (low brilliance) of the generated x-rays, so that the useful x-ray flux through a given sample is quite low. Nevertheless, these groups successfully studied ultrafast melting of GaAs by time-resolved x-ray diffraction[10–15] and demonstrated the principle of time-resolved x-ray absorption in the case of photodissociation of the SF_6 molecule.[16]

Synchrotrons are today the most powerful source of x rays. Synchrotron radiation (SR) is tunable over an extremely large region up to the very hard x-ray regime around 100 keV. However, the temporal resolution (pulse width) is limited to the 30–100 ps range. Furthermore, laser-pump SR-probe experiments depend on the available number of x-ray photons per single pulse at the repetition rate of the exciting laser, which is typically 1 kHz for commercial amplified fs lasers. Therefore, such experiments can use only ca. $10^{-5}-10^{-6}$ of the available photon flux at a synchrotron with its much higher pulse repetition rate of 100–500 MHz. Nevertheless, exploiting SR x-ray pulses in a pump-probe configuration has just recently become a reality in pioneering experiments by the Falcone group.[17,18] In such diffraction experiments, they were able to detect coherent phonons in InSb with the 30 ps pulses of the Advanced Light Source (ALS) in Berkeley, by exploiting an x-ray-sensitive streak camera in jitter-free configuration, thus obtaining a temporal resolution around 2–3 ps in averaging mode.[19]

A recent breakthrough by Schoenlein *et al.* promises near 100 fs hard x-ray pulses to become available soon.[20] Hereby an ultrashort laser pulse copropagates with a selected electron bunch inside a wiggler tuned to the fundamental wavelength of the laser. In the overlap region of ca. 100 fs (or longitudinally ca. 30 μm), the long electron bunch is sliced energetically in two ultrashort parts, which can be spatially separated from the main bunch in a dispersive section of the storage ring, making possible the extraction of *femtosecond* SR pulses. The cross correlation of the visible SR-sliced pulses with the slicing laser itself delivered a pulse width around 160 fs.[20] While the expected flux in the hard x-ray regime is rather low, this source represents the shortest x-ray source with existing technology.

X-ray *diffraction* is a coherent process, in which one uses the long-range order of the sample to retrieve information about local structure. Therefore, in a time-resolved x-ray diffraction experiment, the largest number of centers has to be *coherently* excited by the pump laser. This leads to extreme excitation conditions (high power pump intensities), so that time-resolved diffraction on biological samples has been limited so far to the nanosecond domain,[21] although recently transient structural changes in organic solids on the subnanosecond time scale were reported.[22] For shorter time scales only order–disorder phenomena were reported so far,[6–8,11–15,19,23] e.g., melting, on more robust samples, which permit repeated laser heating. Ideally, it would be more useful to have direct access to the *local* response to photoexcitation, since ultrashort time scales imply ultrashort length scales.

X-ray absorption (XAS) techniques such as extended x-ray absorption fine structure (EXAFS) and x-ray absorption near-edge structure (XANES) spectroscopies deliver local structural information.[24,25] While XANES is more complicated to interpret from a structural point of view, it contains rather simple phenomena like the chemical shift, which describes the oxidation state of the atom.[25] The oscillations that appear in EXAFS are due to the interference between the outgoing photoelectron wave created in the excited center and the wave that is scattered back from the neighboring atoms. The depth of the oscillatory modulation contains information about the backscattering amplitude, which itself depends on the electronic density of the surrounding atoms (thus on their nature) and on the coordination number. Due to the different phase shifts of the different types of atoms one can distinguish between different scatterers. The oscillatory period in k-space of the photoelectron can be Fourier transformed into bond distances. Thus EXAFS delivers a quite detailed picture of the local environment, and interatomic separations can nowadays be determined with an accuracy down to the 100 fm range.[26]

The EXAFS process itself, namely ejection, backscattering at a neighboring atom, and interference with the core-hole initial state, is an extremely fast process. For inner-shell electrons with ionization energies well above 1 keV, this process is mostly completed well within ca. 1 fs, as can be derived from the measured edge widths.[27] This means that EXAFS takes a truly instantaneous snapshot of immobile atoms, even during a violent chemical reaction. Therefore, implementing ultrafast time-resolved EXAFS is not limited by the pump-probe scheme. This was verified by Brown and Wilson[28] in a rigorous theoretical description of time-resolved EXAFS in the case of the excited state dynamics of I_2. In that study, they extended the usual EXAFS function[25] to a time-dependent quantity with the temporal variation resulting from the (photo-triggered) electronic and nuclear dynamics of the system. In a more recent development, Tanaka *et al.* proposed a treatment of time-resolved x-ray spectroscopies in terms of nonlinear response functions and susceptibilities.[29] While these studies clearly show the principle feasibility and the potential of time-resolved EXAFS, they do not quantify their findings with respect to nowadays available ultrashort x-ray sources. It is indeed the instrumental limitations, which currently hamper the implementation of this new technique.

As mentioned above, to date the only ultrafast time-resolved XAS experiment was performed by the Wilson and Kieffer groups.[16] In this experiment, gaseous SF_6 was photolyzed with an intense optical laser pulse, and a subsequent continuum x-ray pulse from a laser-driven x-ray plasma source probed the XAS in the XANES region of the sulphur K edge. While the noise on the spectrum was still too large to observe the K edge jump itself, the disappearance of the SF_6 shape resonance (which occurs upon dissociation) was clearly observed. The absorption cross section of this shape resonance exceeds that of the sulphur K edge by nearly an order of magnitude,[30] which is the main reason for the suc-

cess of this experiment. Recently a time-resolved EXAFS study with 14 ns resolution was reported at the Advanced Photon Source APS (Argonne National Laboratory, Chicago).[31] Chen *et al.* measured the ligand dissociation of Ni-TPP, a complex with a Ni center and octahedrically oriented ligands, via Ni K-edge EXAFS, photostimulated by a UV picosecond laser. The change in nearest-neighbor distance from 192 to 210 pm was resolved in this photochemical process. However, data accumulation times of 300 s per data point, adding up to ca. 20 hours for one entire spectrum, were necessary.

With the existing (and still improving) techniques for ultrashort x-ray pulse generation previously mentioned, one has to evaluate the current capabilities to allow structural dynamical research using x-ray absorption. To begin testing the method, we need a simple system with the potential to allow temporal studies on the following time scales: 100 ps (pulse width of modern SR storage rings), 1–10 ps (pulse width of current laboratory-based x-ray sources, and temporal resolution of x-ray streak cameras), and finally the near 100 fs fundamental time scale obtained by ultrafast time-slicing of electron bunches in a storage ring.[20] In addition, not so much are the time scales of the studied dynamics important for establishing this new scheme, but the changes in the x-ray probe absorption cross section following photoexcitation are paramount.

With this in mind, it seems logical to begin with a system promising a large signal before advancing towards the real goal of this emerging research field, namely to exploit time-resolved EXAFS in structural research. Iodide in water offers many of these requirements. In addition, it is an ideal system to investigate electronic solvation dynamics in polar solvents following a dramatic charge redistribution around the solute. We have already presented some of these calculations in letter form;[32] we now treat this system in much greater detail, which also permits us to generalize the results for other systems. In the following, we will review its properties (x-ray spectroscopy and optically photoinduced dynamics), before proceeding to the calculation of the expected signal with an existing pulsed x-ray source.

II. THE SYSTEM

One fascinating goal for implementing time-resolved XAS techniques is to monitor the solvent–solute dynamics in disordered media. Photoionization of single aqueous ions promises a rather large structural rearrangement due to the close proximity of the caging solvent. Halide ions appear for this purpose as an attractive solute. Our choice for the system consisting of I^- in H_2O solvent is based on the following criteria:

(i) The presence of strong near-edge x-ray absorption lines[33] and of well-known static x-ray absorption spectra of iodine compounds. These have been complemented by our own measurements which are presented later in this work.

(ii) A long enough lifetime (several hundred ps) of the neutral I atoms in the H_2O solvent based on the decay times of the solvated electron after its abstraction,[34] thus the I atoms can be probed with the conventional time resolution available at synchrotrons.

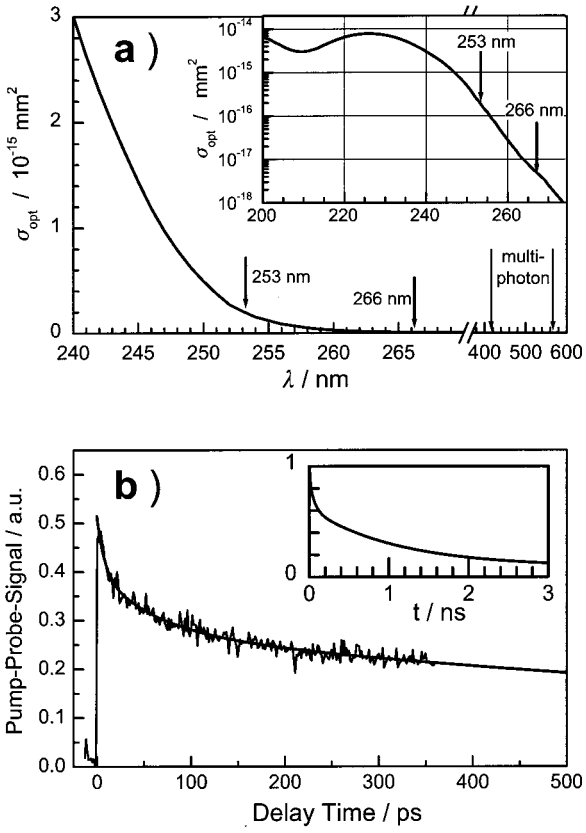

FIG. 1. (a) UV absorption cross section of I^-/H_2O. Photoexcitation into the broad CTTS states (leading to formation of an I^0 radical) can occur via one-photon excitation (e.g., with 253 or 266 nm light from a frequency-tripled Ti-Sapphire laser indicated in the figure), or via two- (or multi-) photon absorption in the visible range (indicated in the figure). The inset displays the same curve on a semi-logarithmic scale. (b) Transient absorption of photogenerated ($\lambda = 400$ nm) solvated electrons in a 2 mol/l LiI/H_2O solution. The solid line is a three-component exponential fit ($\tau_1 = 8$ ps, $\tau_2 = 60$ ps, $\tau_3 = 1$ ns) with fixed constants τ_1 and τ_2 from Ref. 34. The insert displays the expected survival probability for the first 3 ns following photodetachment.

These two points are now discussed in detail in the light of our work and results from the literature, stressing, however, the experimental conditions relevant for time-resolved XAS experiments.

A. Optical studies of the ultrafast dynamics

The absorption spectrum of I^- in water shows two strong and broad UV absorption bands [Fig. 1(a)], centered near 200 and 230 nm, respectively.[35,36] This electronic absorption spectrum has been ascribed to charge-transfer-to-solvent-states (CTTSs). The CTTS excited electron remains localized for ca. 1 ps around the parent atom by the electric field of oriented solvent molecules.[37–41] Excitation of I^- into one of the CTTSs, eventually leads to the formation of an iodine radical via

$$I^- + \hbar\omega(200-270\ \text{nm}) \rightarrow I^0 + e^-.$$

Figure 1(b) shows our femtosecond pump-probe results for two-photon excitation of I^- with 400 nm, 300 fs pulses, and probing with 800 nm, 150 fs pulses. The probe pulses detect only the formation and decay kinetics of the aqueous electron. Similar kinetics were reported by other authors, including direct CTTS excitation with one UV photon.[34] Unfortunately, I^0 has no detectable absorption bands in the optical range, so that in both cases we do not observe the iodine radical directly. We therefore infer the lifetime of the I radical from that of the solvated electron. This is certainly justified for low concentration solutions, while larger concentrations will enhance the diffusion-controlled reaction of iodine atoms with the iodide pool towards I_2^- formation. This process can severely diminish the radical population within the first nanosecond, but will not play a role within the first 10 ps following photolysis. It is these ultrafast processes that we ultimately seek to observe in the experiment, and therefore we will ignore subsequent reactions in the calculations presented later.

Although various experimental[42–46] and theoretical[47–49] studies have been carried out on the halide CTTSs in bulk H_2O as well as in size-selected clusters,[37–41] the dynamical data is still too complicated to allow a definitive description. This comes from different processes overlapping in the otherwise rather simple transient spectra. Ideally, it would be interesting to find a way of detecting the I atom directly. This is possible by x-ray absorption as will be discussed later. From the point of view of dynamics, I^- in water is an interesting system since the nascent radical should still be observed with the rather long SR pulse width in the 30–100 ps range.

B. X-ray absorption by halogen anions

To our knowledge, only very recently has an EXAFS study determining the $I^- - O$ distance of aqueous iodide been reported.[50] This may be due to the fact that x-ray diffraction (diffuse scattering) data on this system with several different cations have been available for a long time,[51] which therefore made accurate EXAFS studies on disordered aqueous systems less attractive. The diffraction data yielded average values for the $I^- - O$ distance in the 360–370 pm range.[52] Similar x-ray diffraction studies on the smaller Br^- in aqueous solution yielded $Br^- - O$ distances in the 330–340 pm range,[52] but recently D'Angelo *et al.* reported a detailed EXAFS study on aqueous bromide.[53] It was shown that the conventional approach in the analysis of EXAFS data, namely describing the coordination of the photoabsorbing atom with a set of Gaussian shells, is too crude to describe the local radial distribution function $g(r)$ accurately. In their study, they started off with a theoretical $g(r)$ distribution from their own molecular dynamics simulations[53] to fit their data, before they refined the input distribution function in the minimization procedure. Further improvements of this method allowed them to measure the first shell distances around Br^- with accuracies well below 10 pm in methanolic solution.[54] These results emphasize the potential of EXAFS for structural studies of disordered systems.

Figure 2(a) shows an overview static XAS spectrum of I^- in H_2O solvent, which we recorded under realistic pump and probe conditions at the bend magnet beam line 7.3.3 of the ALS and at the repetition rate of a commercial amplified fs laser, i.e., 1 kHz. Thus, the spectrum in Fig. 2(a) was obtained by using only one single x-ray pulse every millisecond, which has to be compared to the much larger pulse repetition rate around 500 MHz exploited by the conventional SR user. Electronic gating of the transmitted x-ray pulse train, recorded with a fast x-ray sensitive avalanche photodiode (APD) detector, permits us to single out the selected x-ray pulse. Details of this experimental scheme can be found in Refs. 55 and 56. Note that each data point in Fig. 2(a) represents an accumulation time of 0.1 s, or only 100 single x-ray shots. The measured noise on this spectrum exceeds the statistically expected value by only a factor of ca. 5 and recent improvements by us reduced this penalty down to a factor of below 3.[55] Next to unwelcome but correctable glitches in the spectrum, we can clearly resolve the EXAFS modulations due to the caging water molecules above all three edges. A close up of the region of the L_1 edge is shown in Fig. 2(b), where the EXAFS oscillations are better resolved due to the longer accumulation time, thus demonstrat-

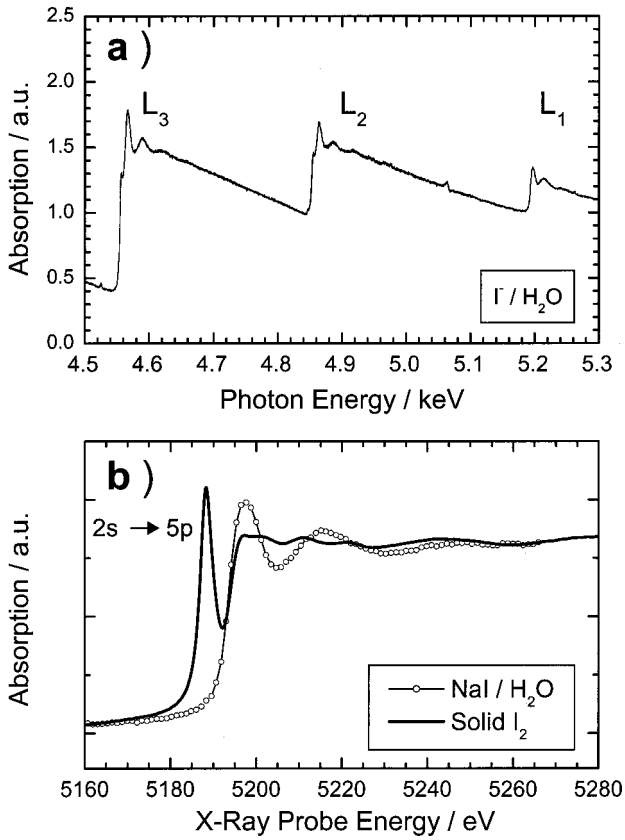

FIG. 2. (a) Overview of the iodine L edges recorded for a 0.1 mm thick free flowing liquid jet at 1 mol/l concentration. Accumulation time per data point is 0.1 s, and only one single x-ray pulse per millisecond is used (thus each data point represents the accumulated dose of 100 single x-ray pulses). (b) Close-up of the L_1 edge for the same sample. This spectrum contains the average of 20 scans with a data accumulation of 1 s per data point for each scan, and again only one x-ray pulse per millisecond is used. A 3 μm thick solid I_2 film (Ref. 57) is displayed for comparison. It shows the intense pre-edge feature ($2s \rightarrow 5p$ transition), which is expected to occur in the iodide spectrum following photodetachment.

ing our current achievements for time-resolved XAS at 1 kHz.

The removal of the electron from I^- results in a $5p$ hole, and a Lorentzian-shaped feature should appear in the preedge region. Thus the appearance of the neutral I atom can, in principle, be observed by measuring the intense $2s \rightarrow 5p$ transition of iodine right below its L_1 edge. A related resonance is observed in molecular I_2 due to the empty (antibonding) σ_u state, which converges to the $(2p)^5$ ground state atoms ($^2P_{1/2,3/2}$) in the dissociation limit. This transition, measured in solid I_2,[57] is also displayed in Fig. 2(b). We expect the preedge resonance of I^0 radicals to be at least as strong as observed for I_2, thus fulfilling our condition of a strong photoinduced probe signal.

Finally, the EXAFS changes are quite large in the case of solvated iodine radicals due to the large coordination number of surrounding O atoms. For the precursor I^-, the EXAFS modulations amount up to ca. 20% of the edge jump [Fig. 2(b)]. Thus, the system is also potentially attractive for a demonstration of time-resolved structural studies using EXAFS. The I–O distance should change considerably upon photodetachment. Values for iodine are currently unknown, but in a theoretical study of aqueous Br radicals the predicted Br–O distance changed from 335 pm for the ion to ca. 280 pm for the neutral radical.[58] Assuming a similar reduction in the iodine–oxygen distances would result in a pronounced change in the EXAFS signal. This fact is illustrated in Fig. 3, where a corresponding theoretical analysis combined with preliminary data sets is presented. Figure 3(a) shows the case of the iodine L_1-edge while Fig. 3(b) depicts the situation for the L_3-edge. The presented experimental data were recorded under realistic pump and probe conditions using 100 ps single x-ray pulses and were collected at the bend magnet beamline 5.3.1 at the ALS. They represent a single scan with 2500 x-ray pulses per data point (accumulation time 2.5 s at 1 kHz). The raw data were processed using EXAFSPAK.[59] Nonweighted EXAFS spectra were obtained after background subtraction, normalization, and transformation into momentum space using threshold energies (for which $k=0$ applies) of 5191 eV (L_1-edge) and 4560 eV (L_3-edge). The radial structure functions [Fig. 3(c)] were obtained by Fourier filtering the normalized EXAFS spectra over the k-range of 2 to ca. 6 $Å^{-1}$ and are presented without phase shift correction. The EXAFS spectra were fitted using least-squares methods. Required phase-shift and amplitude functions were obtained by *ab initio* calculations using FEFF8.[60] For both edges, the EXAFS analysis revealed consistent iodine–oxygen distances (345 ± 7 pm). Compared to results obtained using diffraction techniques,[51,52] our preliminary results indicate a somewhat shorter I–O distance. This result is, however, consistent with the outcome of a recent iodine K-edge EXAFS study.[50] Experimental data and corresponding fits (solid lines) are compared to theoretical calculations (dashed lines) assuming an I–O distance of 300 pm. For the I–O distances of 345 and 300 pm, the EXAFS oscillations are nearly completely out of phase. The present analysis demonstrates the suitability of both the iodine L_1-edge as well as the L_3-edge EXAFS to differentiate between aqueous I^0 and I^- species.

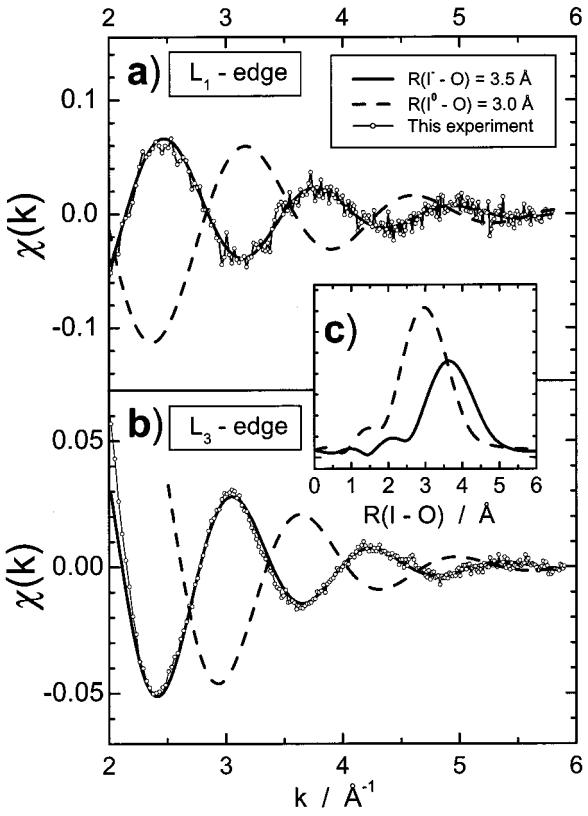

FIG. 3. Experimental EXAFS spectra (dots) and fits (solid lines) of aqueous iodide together with simulations of the expected EXAFS for the nascent iodine radical (dashed) above the iodine L_1 (a) and L_3 (b) edges. (c) Radial distribution functions for the fitted experimental data (solid) and the simulated (dashed) I-O distance for the photogenerated atom.

III. PUMP-PROBE CALCULATIONS WITH ULTRASHORT LASER AND X-RAY PULSES

In time-resolved XAS, the difference in x-ray absorption cross sections between pumped and unpumped species at a given x-ray probe energy governs the outcome and thus the feasibility of the experiment. The time delay between pump and probe pulses, and thus the dynamics of the triggered photochemical reaction, is crucial for observing the pump-probe signal. In the following we treat the pump-probe signal at a fixed time delay, e.g., immediately after excitation. Consequently, the photoinduced x-ray absorption change has to be averaged over the temporal resolution of the experiment. This is ca. 50–100 ps when probing with a single SR pulse, and ca. 100 fs when probing with time-sliced x rays.[20] For the iodide photodetachment experiment, we initially seek to observe the preedge resonance, whose intensity is governed by the amount of surviving radicals.

Once the ultrafast events have been completed (typically within the first few picoseconds), the dynamical behavior can be described by the survival probability, as shown in Fig. 1(b). Therefore, we calculate the pump-probe signal as a function of the photoexcitation process, and utilize the final x-ray absorption cross-section change as a fixed input parameter including the fraction of excited (and surviving) species. Once we have successfully measured the completed reaction in the experiment, we can tackle the problem of studying the

first ultrashort events via time-resolved EXAFS. This will require an increased sensitivity due to the smaller change in x-ray absorption, though the intermediate changes during a photodissociation process, probed via EXAFS, can also exceed the final changes. In the calculations below we assess the feasibility by calculating the signal based on the final (i.e., completely photodetached) state, but including the temporally averaged survival probability.

In the pump-probe experiments, we can describe the transmitted x-ray intensity in dependence of the amount of excited species, thus modifying the Lambert–Beer law with respect to the photoexcitation yield $f(n_{\mathrm{sam}})$. In the following analysis, we use a fixed sample thickness $d=\mathrm{const}$. The calculations are carried out for varying values of the absorption coefficient of I^- in the optical domain. The main adjustable parameter is the sample concentration n_{sam} (in units of particles per mm^3), which in turn affects $f(n_{\mathrm{sam}})$, averaged over d. The photolysis yield $f(n_{\mathrm{sam}})$ depends on the excitation process (thus on the number of incident laser photons per pulse, N_0^{ph}, and on the optical absorption cross section σ_{opt}), which we take into account. We can write the modified Lambert–Beer law of the transmitted x-ray intensity via

$$I_1 = I_0 e^{-n_{\mathrm{sol}}\sigma_{\mathrm{sol}}d} e^{-n_{\mathrm{sam}}\sigma_{\mathrm{cat}}d} e^{-(1-f)n_{\mathrm{sam}}\sigma_{\mathrm{gr}}d} e^{-fn_{\mathrm{sam}}\sigma_{\mathrm{ex}}d} \quad (1)$$

with $n_{\mathrm{sol}}=$ solvent density (in particles/mm^3), $n_{\mathrm{sam}}=$ sample concentration (in particles/mm^3), $\sigma_{\mathrm{sol}}=$ x-ray absorption cross section of a solvent molecule $\sigma_{\mathrm{cat}}=$ x-ray absorption cross section of all impurity particles (e.g., the cations for the I^- photodetachment experiment), $\sigma_{\mathrm{gr}}=$ x-ray absorption cross section of the unpumped sample particle at x-ray energy E_x. $\sigma_{\mathrm{ex}}=$ x-ray absorption cross section of the excited sample particle (at E_x), $f=f(n_{\mathrm{sam}},N_0^{\mathrm{ph}},\sigma_{\mathrm{opt}})=$ photoexcitation yield of the sample particle, $I_0=N_x^0\Phi_{\mathrm{det}}=$ incident x-ray flux corrected for the quantum yield Φ_{det} of the detector, and $N_x^0=$ number of incident x-ray photons on the sample per pulse. Setting $\Delta\sigma_{\mathrm{ex}}=\sigma_{\mathrm{ex}}-\sigma_{\mathrm{gr}}$ we can rewrite Eq. (1) as

$$I_1 = I_0 e^{-n_{\mathrm{sol}}\sigma_{\mathrm{sol}}d} e^{-n_{\mathrm{sam}}(\sigma_{\mathrm{gr}}+\sigma_{\mathrm{cat}})d} e^{-fn_{\mathrm{sam}}\Delta\sigma_{\mathrm{ex}}d}. \quad (2)$$

Equation (2) then describes the transmitted x-ray intensity, I_1, as a function of the optical pump process. The third term containing the photolysis yield f defines the contribution of the pumped species to the total transmitted intensity, thus the pump-probe signal. We can define a useful signal in this pump-probe process as the difference signal in transmission between pumped (I_1^{pum}) and unpumped (I_1^{unp}) sample,

$$S = I_1^{\mathrm{pum}} - I_1^{\mathrm{unp}}, \quad (3)$$

with the pumped and unpumped transmission defined via Eq. (2) with and without ($f=0$) photoexcitation yield f. The shot noise is defined via single photon counting statistics, thus

$$N = \sqrt{I_1^{\mathrm{pum}} + I_1^{\mathrm{unp}}}. \quad (4)$$

The ratio between Eqs. (3) and (4) finally defines the signal-to-noise ratio S/N, which we seek to maximize in the experiment. Mathematically, we find the optimum experimental conditions, e.g., the optimum sample concentration, by finding the extreme value in

$$\frac{d}{dn_{\mathrm{sam}}} S/N = 0. \quad (5)$$

In Eq. (2) we identify three contributions:

$$I_{\mathrm{sol}} = I_0 e^{-n_{\mathrm{sol}}\sigma_{\mathrm{sol}}d}, \quad (6)$$

$$gr(n_{\mathrm{sam}}) = e^{-n_{\mathrm{sam}}(\sigma_{\mathrm{gr}}+\sigma_{\mathrm{cat}})d}, \quad (7)$$

$$ex(n_{\mathrm{sam}}) = e^{-n_{\mathrm{sam}}f\Delta\sigma_{\mathrm{ex}}d}. \quad (8)$$

Equation (6) describes the transmission of the neat solvent, and does not influence the optimum sample concentration, as derived via Eq. (5). As expected, it only influences the achievable S/N value. The ground state [Eq. (7)] and the excited state [Eq. (8)] contributions are sample concentration dependent, and Eqs. (7) and (8) determine the best sample concentration following Eq. (5) to perform the pump-probe experiment at a given sample thickness d. Obviously, for $f=0$ we gain the stationary solution of the Lambert–Beer law (simple transmission through a sample). In view of the optimum sample concentration (for the largest S/N ratio) for the stationary absorption case [via Eq. (5) and $f=0$], we find that even larger concentrations n_{sam} for the pump-probe experiment will suffer in S/N, even for $f=1$. This will be demonstrated in more detail in Sec. IV.

Now we consider the photolysis yield $f(n_{\mathrm{sam}},N_0^{\mathrm{ph}},\sigma_{\mathrm{opt}})$. For one-photon absorption processes, we calculate the fraction f of sample particles which have been excited by the pump source, *averaged* over the constant thickness d of the sample, via the ratio of absorbed laser photons after the sample thickness d and the absolute number of sample particles in the illuminated volume $F\cdot d$, and obtain

$$f(n_{\mathrm{sam}},N_0^{\mathrm{ph}},\sigma_{\mathrm{opt}}) = \frac{N_0^{\mathrm{ph}}}{n_{\mathrm{sam}}Fd}(1-e^{-n_{\mathrm{sam}}\sigma_{\mathrm{opt}}d}) \quad (9)$$

with $N_0^{\mathrm{ph}}=$ number of incident laser photons per pulse, $d=$ sample thickness, $F=$ focal area illuminated by the laser, and $\sigma_{\mathrm{opt}}=$ optical absorption cross section of the sample particle.

Ideally, F should have the size of the x-ray probe focus, and typical foci diameters are in the 100–200 μm range. For the proposed experiments we use a liquid jet, and $d=0.1$ mm is therefore a typical value. Equation (9) is only valid when neglecting solvent and impurity absorption in the optical domain. In our experiments, NaI is the precursor of the I^- species. While Na^+ impurity absorptions do not interfere with the I^- photoexcitation, multiphoton absorptions of the solvent (e.g., H_2O) decrease the possible optical excitation.[61] However, since we use $\geqslant$30 ps x-ray probe pulses in the experiment, we can stretch the laser pulse width until multiphoton absorptions become negligible.

Applying $f=1$ (thus complete photoexcitation) in Eq. (2), we can calculate the best sample concentration for obtaining the lowest noise level via Eq. (5), and thus quantify the best possible signal-to-noise ratio ($=S/N$) under realistic conditions (e.g., the x-ray photon flux). This strongly aids in selecting possible experiments and allows us to assess the potential for success of a proposed EXAFS structural dynamics experiment under realistic pump and probe conditions. The photoexcitation term, Eq. (8), contains the product

of f and $\Delta\sigma_{ex}$, which governs the S/N ratio. To account for ultrafast recombination processes as well as to include averaging the probe pulse width over the observed dynamics, we can introduce a factor Φ_{yield} in Eq. (9). With this correction, we thus account for the limited survival probability observed for I radicals of ca. 25%–50%.

However, this assumes no principle changes for the averaged probe signal, except in intensity due to the decreasing surviving population, i.e., no changes in the XAS shape are taken into account, which may not be fully valid when examing averaged bond distances via EXAFS. In this case, we would have to include all possible bond distances occurring within the probe pulse width. However, for the case treated here of the photogenerated preedge resonance in the initial XANES experiment, only intensity reduction is expected to occur over the SR probe pulse width.

IV. RESULTS AND DISCUSSION

In the following we present the calculations using realistic input parameters. We then calculate the optimum conditions for performing these experiments as a function of the pump parameters and determine the time necessary for shot-noise limited data acquisition. The input parameters are the following. $N_x^0 = 10^4$ is the number of incident monochromatic x-ray photons per pulse at a given photon energy E_x with bandwidth $\Delta E_x/E_x \cong 0.1\%$. This value represents the expected flux from both the 100 ps single pulses from an ALS bend magnet in the 2–10 keV range,[55,62] and is close to the value expected for 100 fs x-ray pulses extracted from a proposed extraction undulator using the time-slicing scheme.[20,63] For 100 fs sliced x-ray pulses extracted at the current beamline 5.3.1, we can assume ca. 1–10 monochromatic x-ray photons per pulse. $\Phi_{Det} = 0.75$ is the quantum efficiency of the x-ray detector used in these calculations. Its value is quite comparable to the efficiency of a commercial x-ray sensitive avalanche photodiode in the 5 keV range. $F = 0.1 \times 0.2\ mm^2$ is the area of focal overlap between two congruently focused laser and x-ray beams (which thus have the same individual foci sizes). $d = 0.1$ mm.

First we consider the case of simply optimizing the sample concentration, when all other parameters are fixed, like sample thickness and optical absorption cross section. Figure 4 illustrates this for different laser pulse energies for the iodide photodetachment experiment at $\lambda = 253$ nm (or $\sigma_{opt} = 2 \times 10^{-16}\ mm^2$). Depending on the available number of exciting laser photons the optimum sample concentration increases gradually with increasing laser pulse energy. However, since the number of x-ray photons for probing the dynamics is finite, the optimum sample concentration even for infinite incoming laser photons is limited (here 2.1 mol/l for $d = 0.1$ mm), because higher concentrations (although resulting always in full photoactivation) decrease the transmitted x-ray intensity, and thus the achievable S/N value (inset in Fig. 4). In a real experiment, the laser wavelength can be tuned over a wide region from the IR to the deep UV, which can thus be absorbed by the same species, though with wavelength-dependent optical absorption cross sections. On the other hand, laser pulse energies are largest for certain

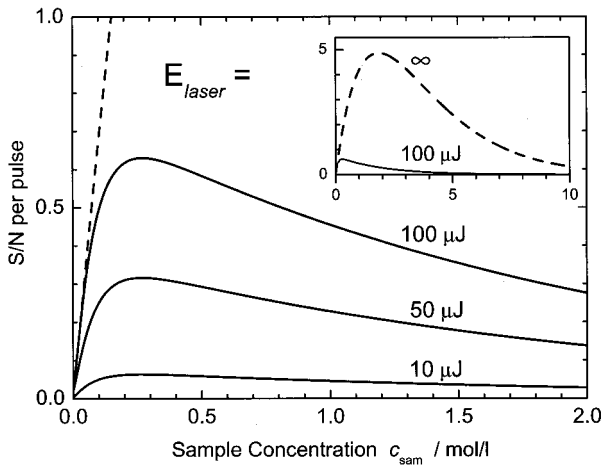

FIG. 4. Signal-to-noise ratio S/N for one pump-probe cycle as a function of sample concentration c_{sam} for a fixed thickness $d = 0.1$ mm and a laser pump wavelength of $\lambda = 253$ nm. The S/N value is roughly proportional to the laser pump energy for realistic laser pump energies ($E_{laser} = 10$, 50, 100 μJ as indicated in the figure), while the optimum sample concentration varies little. The inset displays the best possible case for this system assuming infinite laser photons (dashed curve) together with the case for $E_{laser} = 100\ \mu$J for comparison.

fixed wavelengths (e.g., 800, 400, and 266 nm, with respectively decreasing intensities for Ti–sapphire lasers). Choosing the best laser wavelength for a given experiment results from a careful calculation of the S/N value as a function of available laser pulse energy and optical absorption cross section at the selected laser wavelength. Therefore, it makes sense to present the following results as a function of the optical absorption cross section in order to account for the tunability of the laser pump source.

Repetition rate for the pump-probe experiments is set to either 1 or 5 kHz, which represent the current values for both interfaced fs lasers at beamline 5.3.1 of the ALS.[63] With these input parameters, we can assess the feasibility of different time-resolved XAS experiments quite reliably, since we have used rather conservative values. The S/N value after m shots increases with $(m)^{1/2}$, as can be seen from Eqs. (2)–(4) including shot-noise statistics. $1/(S/N)^2$ is thus the number of shots to achieve $S/N = 1$, and the required accumulation time for achieving $S/N = 1$ can be calculated with the repetition rate f_{rep} of the experiment (of the exciting laser) via

$$t = \frac{1}{f_{rep}(S/N)^2}. \tag{10}$$

In Figs. 5–8 we have collected some of the results for the I^- photodetachment experiment, probing the nascent radical by the $2s \rightarrow 5p$ transition just below the iodine L_1-edge. With $N_0^{ph} \cong 10^{14}$ laser photons per pulse (corresponding to 100 μJ pulse energy at 253 nm), Figs. 5 and 6 display the σ_{opt}-dependencies on c_{sam}, the change in transmitted intensity due to photoexcitation, $\Delta I/I$, $f(c_{sam})$, and finally S/N per pump-probe shot using the aforementioned 10^4 x-ray probe photons per pulse. The sample concentration for obtaining the largest S/N varies as a function of the parameters governing the photoexcitation process, N_0^{ph}, and

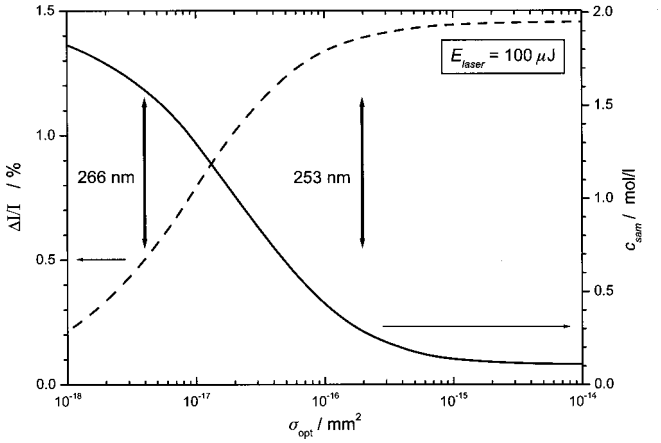

FIG. 5. Results of the calculations for determining the best conditions yielding the largest sensitivity for the iodide photodetachment experiment observed via time-resolved XAS. The arrows indicate the values for experiments performed at the indicated excitation wavelengths. Optimum c_{sam} and resulting change in transmitted intensity, $\Delta I/I$, as a function of σ_{opt} with a laser pulse energy of 100 μJ.

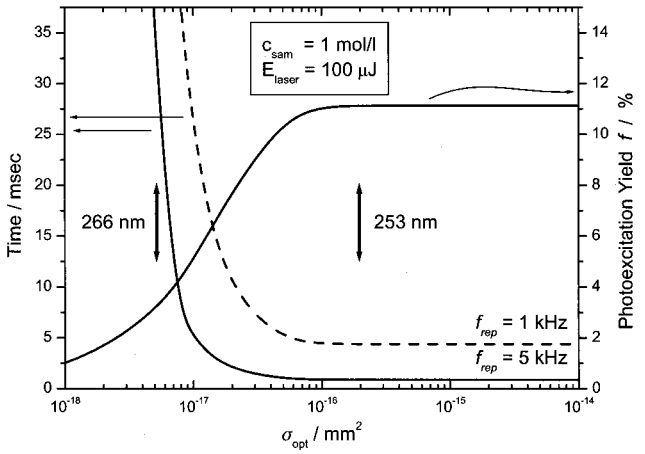

FIG. 7. Data accumulation time at $f_{\mathrm{rep}}=1$ kHz and f as a function of σ_{opt} for an incident x-ray intensity of 10^4 photons per pulse, and fixed concentration and laser pulse energy. The arrows denote the optical cross sections for the indicated laser pump wavelengths.

σ_{opt}. This interplay is shown in Fig. 5 for E_{laser} fixed to 100 μJ. Therefore, the other curves were derived using this dependence $n_{\mathrm{sam}}(\sigma_{\mathrm{opt}})$ as input. For σ_{opt} values smaller than the x-ray absorption cross sections $(\sigma_{\mathrm{gr}}+\sigma_{\mathrm{cat}})$, n_{sam} is rather large (here $c_{\mathrm{sam}}\cong 2$ mol/l). We would obtain the same result when optimizing the sample to measure the static ground state absorption cross sections $(\sigma_{\mathrm{gr}}+\sigma_{\mathrm{cat}})$. In the limit of very low σ_{opt} (as compared to $\sigma_{\mathrm{gr}}+\sigma_{\mathrm{cat}}$), we use too few pump laser photons for the excitation process (since the laser transmission is high). This cannot be compensated by simply increasing the concentration, since then the probe beam would be nearly completely absorbed (i.e., no signal). This would similarly hold for fluorescence detection, if we have to deal with a static fluorescence background.

For increasing σ_{opt} the optimum sample concentration decreases until it converges to a limiting value. In the limit of very large σ_{opt}, the sample absorbs nearly every exciting laser photon, and the limiting value is found to fulfill the equality

$$n_{\mathrm{sam}}Fd=N_0^{\mathrm{ph}} \tag{11}$$

between the number of sample species in the illuminated volume and the number of incident laser photons per pulse. For $N_0^{\mathrm{ph}}=10^{14}$ and $Fd=2\times10^{-3}$ mm^3 we gain $c_{\mathrm{sam}}=0.1$ mol/l in agreement with Fig. 5. The variation of n_{sam} with σ_{opt} is thus found within two boundaries: Low σ_{opt} values necessitate the optimal static sample concentration, while large σ_{opt} values limit the sample concentration via Eq. (8) by the number of incident laser photons. Therefore, in a pump-probe experiment, one can always limit the sample concentration within these boundaries.

We also see in Fig. 6 that for $\sigma_{\mathrm{opt}}\geqslant 10^{-16}$ mm^2 S/N is already only ca. 10%–20% below its best possible value, although we have only excited ca. 30% of the total sample. This results from the fact that for these σ_{opt} values we have already approached total absorption of the exciting laser

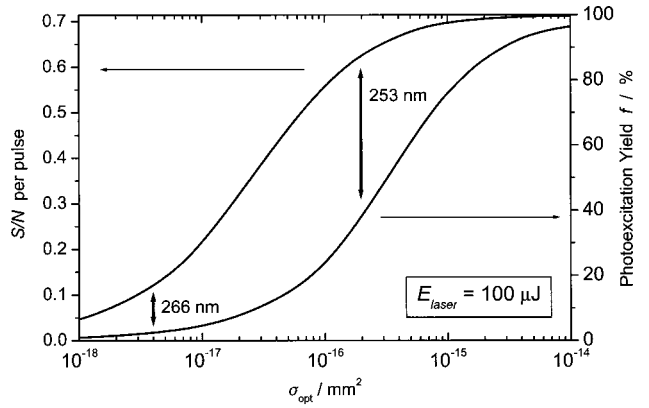

FIG. 6. Photoexcitation yield f and S/N per pump-probe shot as a function of σ_{opt} using $c_{\mathrm{sam}}(\sigma_{\mathrm{opt}})$ (shown in Fig. 6) for a laser pulse energy of 100 μJ and 10^4 incident x-ray photons per pulse.

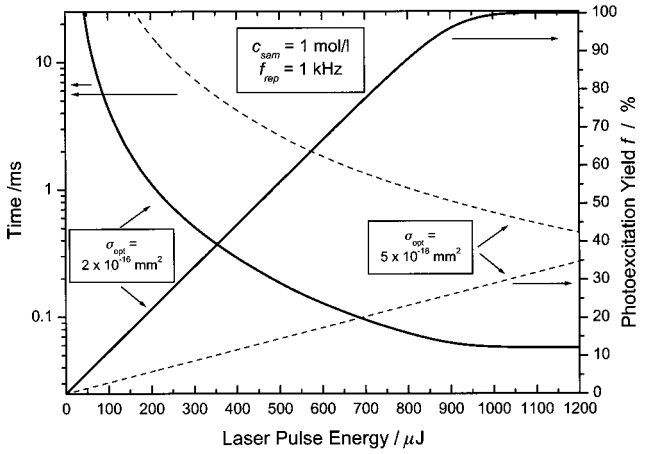

FIG. 8. Data accumulation time (for 10^4 incident x-ray photons per pulse at 1 kHz repetition rate) and photoexcitation yield as a function of incident laser pulse energy (neglecting nonlinear absorptions) for two selected laser wavelengths $(\lambda=253$ nm: $\sigma_{\mathrm{opt}}=2\times10^{-16}$ mm$^2)$, $(\lambda=266$ nm: $\sigma_{\mathrm{opt}}=5\times10^{-18}$ mm$^2)$.

TABLE I. Results of the calculations for the I^- photodetachment experiment with $E_{laser}=100\ \mu J$ per pulse (ca. 10^{14} photons at 253 nm) recorded via time-resolved XAS in transmission mode. ΣN^x describes the required number of accumulated x-ray photons to gain $S/N=1$, and I_x denotes the pulse intensities of two selected x-ray sources (pulse widths indicated).

Edge	Iodine L_1 (5.2 keV)				Iodine L_3 (4.5 keV)	
λ_{laser} (nm)	253		266		253	266
XAS method	XANES	EXAFS	XANES	EXAFS	EXAFS	EXAFS
Max. signal[a]	100%	<10%	100%	<10%	<10%	<10%
c_{sam} (mol/l)	0.27	0.26	1.59	1.44	0.27	1.61
$f(\sigma_{opt}(\lambda), c_{sam}, N^{ph}{}_0)$	37%	38%	2.66%	2.72%	37%	2.65%
S/N per shot[b]	0.63	≤0.062	0.14	≤0.013	≤0.27	≤0.059
ΣN^x	2.5×10^4	$>2.5\times10^5$	5×10^5	$>6\times10^7$	$>1.4\times10^5$	$>2.8\times10^6$
I^x (100 ps)[c]	2×10^4/(pulse 0.1% bandwidth)					
I^x/(100 fs)[d]	1×10^2/(pulse 0.1% bandwidth)					

[a]Relative to the absorption edge jump itself after full photolysis. For EXAFS we have to record two to three oscillations, which accordingly decrease in amplitude. The largest absorption change near $k=2.5\ Å^{-1}$ amounts to ca. 15%, while the third oscillation exhibits a change near 1% (see Fig. 3).

[b]For 10^4 x-ray probe photons per pulse.

[c]Measured effective flux per pulse at beamline 5.3.1 (ALS—Berkeley) under pump-probe conditions at 1 kHz (Refs. 55 and 62).

[d]Expected flux for a new extraction undulator for beamline 5.3.1. The repetition rate for femtosecond experiments will be 40 kHz (Ref. 63).

pulse. Therefore, we cannot further increase the absolute density of excited species by further increasing σ_{opt}, and therefore S/N increases marginally, when approaching 100% photolysis with even larger optical cross sections. We can estimate the cross section σ_{opt}, for which even larger values do not result in an improvement in the experiment, via

$$\frac{N_0^{ph}}{F}=\frac{1}{\sigma_{opt}}, \tag{12}$$

which yields $\sigma_{opt}\cong 2\times10^{-16}\ mm^2$ for the input parameters given above. Equation (12) also describes the condition for achieving complete photoexcitation of the front surface of the sample.

In a real experiment, we usually work at a constant concentration and tuning the laser wavelength allows us to select a certain σ_{opt} value. Figures 7 and 8 are adapted to this case for $c_{sam}=1$ mol/l. This value was chosen from Fig. 5 to represent a medium value within the aforementioned boundaries. The S/N values were converted into data accumulation time via Eq. (10). The optical absorption cross sections for I^-/H_2O at $\lambda=253$ nm ($\sigma_{opt}=2\times10^{-16}\ mm^2$) and at $\lambda=266$ nm ($\sigma_{opt}=5\times10^{-18}\ mm^2$) are indicated by arrows in Fig. 7, and are treated separately in Fig. 8. These wavelengths correspond to the third harmonic of a typical Ti–Sa laser oscillator (fundamental at 800 or 760 nm). A repetition rate of $f_{rep}=5$ kHz was included in Fig. 7 to demonstrate the capabilities of the current fs slicing laser at beamline 5.3.1.

For a cross section of $2\times10^{-16}\ mm^2$ (corresponding to $\lambda=253$ nm for I^- photoionization indicated by the arrow in the figure), we excite 11% of all ions with a 100 μJ laser pulse (Fig. 7). The required data accumulation time at 1 kHz repetition rate for achieving $S/N=1$ is 4.4 ms (or ca. 5 pump-probe shots). In this example, we have already reached the plateau for the highest degree of excitation as a function of σ_{opt}. A more optimum choice of $c_{sam}=0.27$ mol/l (see Fig. 5) would allow us to further increase the photoexcitation yield up to 38%. Nevertheless, S/N increases only by a factor of 1.32, which would reduce the data accumulation time by less than a factor of 2. This results from the arguments given earlier that conditions yielding nearly total absorption of the exciting laser pulse already deliver quite optimal S/N values. Figure 8 displays both the photoexcitation yield and the required accumulation time at 1 kHz for two selected optical absorption cross sections: $2\times10^{-16}\ mm^2$ for 266 nm and $5\times10^{-18}\ mm^2$ (253 nm). Both cross sections are also interesting, since their values are either much larger, or lower, respectively, than the x-ray absorption cross sections. Here, with $c_{sam}=$const, we find a strictly-linear increase of S/N with photoexcitation yield f, which itself increases strictly linearly with laser pulse energy E_{laser}. As soon as the laser saturates ($f=1$) the sample, we reach the limiting value of S/N. Below saturation, we observe the linear dependence of f on E_{laser} in accordance with Eq. (12), when n_{sam} is set constant. If we continuously vary n_{sam} with σ_{opt}, as done in Fig. 5 to optimize the experiment, the linearity of S/N with f or N_0^{ph} is no longer valid, as soon as the optimal conditions allow nearly complete absorption of the exciting laser pulse.

Table I compiles our main results for recording time-resolved XAS during the iodide photodetachment process. The different possible measurements are examined as a function of the input parameters. At the L_1 edge, we can attempt to measure the preedge resonance in the XANES region, which should exhibit the largest possible pump-probe change. The two laser wavelengths describe the frequency-tripled output from a commercial femtosecond laser (266 nm) and the frequency-tripled output from the time-slicing laser at beamline 5.3.1. For time-resolved EXAFS, we have also included the L_3 edge with its much larger edge jump, which facilitates its observation. The optimum concentrations are then calculated as well as the expected photoexcitation yield. The S/N ratio per pulse for an x-ray source of 10^4 photons per pulse is displayed. However, the required number of accumulated x-ray photons per data point to

achieve $S/N=1$ is more useful, since this allows us to assess easily the overall feasibility as a function of the utilized x-ray probe source. Two values are given in the last two rows of Table I, one describing the current 100 ps pulse intensities at a bend magnet beamline, the other describing the expected flux from an improved femtosecond beamline exploiting the time-slicing scheme. Including the repetition rates of both sources in pump probe experiments implies the feasibility of such experiments, since the data accumulation times do not considerably exceed the 1 s level. The expected flux from the current time-sliced bend magnet source 5.3.1, however, amounts to only ca. 10^3-10^4 s^{-1}. This flux poses a great challenge for time-resolved EXAFS, but some time-resolved XANES experiments, including those described in this article, seem feasible.

The main points which follow from these calculations are the following:

(a) Implementing time-resolved x-ray absorption spectroscopy with an ultrafast laser as the pump source is possible with existing pulsed x-ray sources. However, great care must be given to the design of the experiment in order to maximize the utility of the low fluxes from either SR sources or laser-driven x-ray continuum plasma sources. This will govern the overall applicability of this method for the coming years, until extremely brilliant and powerful x-ray free electron lasers (X-FELs)[64] come into user operation. The above calculations allow us to assess the feasibility of a wide class of ultrafast structural dynamics research. While simple condensed phase systems are clearly within reach with existing pulsed x-ray sources, structural dynamics on complex systems like biomolecules in physiological media is much more challenging. Time-resolved EXAFS on the nanosecond time scale with SR has just now been demonstrated on hemelike porphyrin derivatives in solution,[31] however, many *hours* accumulation time were required to access the desired structural information. The above calculations can serve as a guide to optimize the boundary conditions.

(b) In a real experiment on the presented model system, I^- photodetachment in water, we have to include realistic technical limitations, e.g., the overlap between laser and x-ray beams were assumed congruent and rectangular in their spatial profile. The laser and x-ray beams are rather Gaussian shaped and the x-ray focus is elliptical (ca. 150×300 μm v $\times$h). Simply imaging the laser to a circular focus will thus lead to a reduction in sensitivity with respect to the above calculations, which can even exceed an order of magnitude.

(c) Nonlinear effects, most importantly the undesired solvent absorption, are another major contribution to a reduced pump-probe signal. This is because we seek to carry out femtosecond resolved experiments, which in turn demand quite high laser intensities in the 1 TW/cm^2 region. This can lead to a further order of magnitude in sensitivity loss. Therefore, poor design of the experiment can already lead to an inconclusive experiment, even when the calculations indicate otherwise.

(d) This new technique includes many experimental parameters, of which each by itself may not appear significant, but all together can push the experiment out of the feasibility range. In this context we have discovered the importance of noise reduction on the gated x-ray signal. We have currently achieved a noise level exceeding the x-ray shot noise limit by a factor of less than 3, which is close to optimum when considering that an avalanche photodiode has its own intrinsic noise sources. However, with the same detectors and experimental arrangement we have also observed noise distributions at other x-ray beamlines exceeding the shot noise level by two to three orders of magnitude. This corresponds to an effective x-ray flux reduction by 10^4 to 10^6!

The technical implication and its potential are dealt with elsewhere,[55] and the limitations can, in principle, be overcome. The present study aims at delivering guidelines to judge the feasibility of selected time-resolved XAS experiments. For this purpose, the optical and x-ray absorptions, which are the main ingredients, already deliver a detailed understanding of the technical feasibility. The model system presented here can serve as a test bench for implementing structural dynamics in condensed phase chemical systems.

V. CONCLUSIONS

Time-resolved structural dynamics is a new experimental technique, which will complement conventional femtochemical experiments with optical lasers. While still in its infancy, the presented calculations already imply its feasibility with existing ultrashort x-ray sources. In view of the ultrafast x-ray sources and novel source concepts currently under construction or in the planning stage, the optimum use of these instruments becomes more and more important. In this sense the presented calculations demonstrate the high potential as well as the technical limitations of this method.

In this context, we have attempted to apply the model calculations presented here to the previously described time-resolved EXAFS experiment by Chen *et al.* on Ni–TPP.[31] However, without precise knowledge of their experimental details (x-ray flux, sample dimension, x-ray fluorescence detector yield) we cannot satisfactorily simulate this experiment, but we can make reasonable estimates. Indeed, assuming the collection of all emitting Ni K fluorescence photons in a 1–10 mm thick sample at their chosen 1 mmol/l concentration, and recording the EXAFS with 1% noise relative to the edge yields on the order of $10^{10}-10^9$ required incoming x-ray photons per data point, which, according to Ref. 31, occurred over a 300 s period. A reasonable guess for the monochromatic x-ray flux at their wiggler-beamline may be 10^{12} s^{-1}. Therefore, including the flux reduction of 5.5×10^{-4} for pump probe experiments at 1 kHz[31] and the data accumulation time we can assume that they accumulated ca. 10^{11} incoming x-ray photons per data point. Still the correction for the solid angle of the fluorescence detector is missing in our calculation (and we have disregarded reabsorption losses of the fluorescence), which could easily account for the remaining discrepancy towards experiment of one to two orders of magnitude. Thus we gain reasonable agreement with their reported results. This supports the quantitative validity of our calculations as well as their overall applicability to other systems for structural dynamics research.

The described model system will aid in our understanding of environmental effects on photochemical reactions in

the liquid phase. Kloepfer *et al.*,[46] e.g., pointed out the similarity of the observed dynamics in multi-photon ionized water and via the lowest CTTS of solvated iodide. Therefore, complementary information is required to determine the locality of the nascent electron immediately following its liberation from the parent atom.

Ultrafast time-resolved EXAFS has just this potential, although it cannot resolve the liberated electron directly. With the knowledge of the nearest neighbors of the nascent radical, we could infer the structure and dynamics of the CTTS electron, thus allowing us for the first time to complete the picture of this reaction. While only MD simulations of the prognosed ionization mechanism (in combination with the experimental electron spectra) allows us to generate a detailed view of the solvent–solute dynamics, a pump-probe experiment with a hard x-ray probe pulse is capable of monitoring the local environment around the parent ion. Moreover, since optical probe pulses cannot easily access transitions of the nascent halogen radical (but only the liberated electron), x-ray probing is even more appropriate to observe the radical formation in real time. Monitoring the environment of the parent species during the photodetachment process will allow us to distinguish between the different possible ejection channels, thus completing the picture derived from laser-optical experiments. With 100 fs x-ray pulses soon available at the ALS, we can now imagine observing the ultrafast response of the solvent cage due to impulsive electron removal.

ACKNOWLEDGMENTS

This work was funded by the Swiss National Science Foundation (FNRS) via contracts No. FN52561.97 and FN59146.99, by the Paul Scherrer Institut (Villigen, Switzerland), and by the Advanced Light Source (ALS)—Berkeley (USA). The authors thank Phil Heimann and Bob Schoenlein from the ALS—Berkeley for many fruitful discussions as well as for their support during the beamtime periods at the ALS. The authors are indebted to the late Kent R. Wilson for sharing his inspiring ideas towards this fascinating new research area.

[1] A. H. Zewail, Angew. Chem. Int. Ed. Engl. **39**, 2665 (2000); J. Phys. Chem. A **104**, 5660 (2000).
[2] J. C. Williamson, J. Cao, H. Ihee, H. Frey, and A. H. Zewail, Nature (London) **386**, 159 (1997).
[3] J. Cao, H. Ihee, and A. H. Zewail, Proc. Natl. Acad. Sci. U.S.A. **96**, 338 (1999).
[4] H. Ihee, J. Cao, and A. Zewail, Angew. Chem. Int. Ed. Engl. **40**, 1532 (2001).
[5] H. Ihee, V. A. Lobastov, U. M. Gomez, B. M. Goodson, R. Srinivasan, C.-Y. Ruan, and A. H. Zewail, Science **291**, 458 (2001).
[6] T. Anderson, I. V. Tomov, and P. M. Rentzepis, J. Chem. Phys. **99**, 869 (1993).
[7] P. Chen, I. V. Tomov, and P. M. Rentzepis, J. Chem. Phys. **104**, 10001 (1996).
[8] I. V. Tomov, D. A. Oulianov, and P. M. Rentzepis, J. Phys. Chem. B **103**, 7081 (1999).
[9] J. Yu, Z. Jiang, J. C. Kieffer, and A. Krol, Phys. Plasmas **6**, 1318 (1999).
[10] T. Guo, C. Rose-Petruck, R. Jiminez, F. Ráksi, J. A. Squier, B. C. Walker, K. R. Wilson, and C. P. J. Barty, Proc. SPIE **3157**, 84 (1997).
[11] C. W. Siders, A. Cavalleri, K. Sokolowski-Tinten *et al.*, Science **286**, 1340 (1999).
[12] P. Gallant, Z. Jiang, J. Fuchs *et al.*, Proc. SPIE **3157**, 44 (1998).
[13] C. Rose-Petruck, R. Jimenez, T. Guo *et al.*, Nature (London) **398**, 310 (1999).
[14] C. Rose-Petruck, R. Jimenez, T. Guo *et al.*, Nature (London) **398**, 310 (1999).
[15] A. Cavalleri, C. W. Siders, F. L. H. Brown, D. M. Leitner, C. Tóth, J. A. Squier, C. P. J. Barty, and K. R. Wilson, Phys. Rev. Lett. **85**, 586 (2000).
[16] F. Ráksi, K. R. Wilson, Z. Jiang, A. Ikhlef, C. Y. Côté, and J.-C. Kieffer, J. Chem. Phys. **104**, 6066 (1996).
[17] J. Larsson, Z. Chang, E. Judd *et al.*, Opt. Lett. **22**, 1012 (1997).
[18] J. Larsson, A. Lindenberg, P. A. Heimann, P. H. Bucksbaum, R. W. Lee, J. S. Wark, and R. W. Falcone, Appl. Phys. A: Mater. Sci. Process. **66**, 587 (1998).
[19] A. M. Lindenberg, I. Kang, S. L. Johnson *et al.*, Phys. Rev. Lett. **84**, 111 (2000).
[20] R. W. Schoenlein, S. Chattopadhyay, H. H. W. Chong, T. E. Glover, P. A. Heimann, C. V. Shank, A. Zholents, and M. Zolotorev, Science **287**, 2237 (2000).
[21] V. Srajer, T. Y. Teng, T. Ursby *et al.*, Science **274**, 1726 (1996).
[22] S. Techert, F. Schotte, and M. Wulff, Phys. Rev. Lett. **86**, 2030 (2001).
[23] C. Rischel, A. Rousse, I. Uschmann *et al.*, Nature (London) **390**, 490 (1997); A. Rousse, C. Rischel, S. Fourmaux *et al.*, *ibid.* **410**, 65 (2001).
[24] E. A. Stern and S. M. Heald, in *Handbook on Synchrotron Radiation*, edited by E. E. Koch (North-Holland, Amsterdam, 1983), Vol. 1B, p. 955 ff.
[25] B. K. Agarwal, *X-Ray Spectroscopy* (Springer, New York, 1991).
[26] U. Buontempo, A. Filipponi, P. Postorino, and R. Zaccari, J. Chem. Phys. **108**, 4131 (1998).
[27] M. O. Krause, J. Phys. Chem. Ref. Data **8**, 307 (1979).
[28] F. L. H. Brown, K. R. Wilson, and J. Cao, J. Chem. Phys. **111**, 6238 (1999).
[29] S. Tanaka, V. Chernyak, and S. Mukamel, Phys. Rev. A **63**, 063405 (2001).
[30] J. L. Dehmer, J. Chem. Phys. **56**, 4496 (1972).
[31] L. X. Chen, W. J. H. Jäger, G. Jennings, D. J. Gosztola, A. Munkholm, and J. P. Hessler, Science **292**, 262 (2001).
[32] C. Bressler, M. Saes, M. Chergui, R. Abela, and P. Pattison, Nucl. Instrum. Methods Phys. Res. A **467–468**, 1444 (2001).
[33] See, e.g., N.-G. Park, S.-W. Cho, and S.-J. Kim, Chem. Mater. **8**, 324 (1996).
[34] J. A. Kloepfer, V. H. Vilchiz, V. A. Lenchekov, and S. E. Bradforth, Chem. Phys. Lett. **298**, 120 (1998).
[35] L. I. Grossweiner and M. S. Matheson, J. Phys. Chem. **61**, 1089 (1957).
[36] J. Jortner, M. Ottelenghi, and G. Stein, J. Phys. Chem. **68**, 247 (1964).
[37] D. Serxner, C. E. H. Dessent, and M. A. Johnson, J. Chem. Phys. **105**, 7231 (1996).
[38] L. Lehr, M. T. Zanni, C. Frischkorn, R. Weinkauf, and D. M. Neumark, Science **284**, 635 (1999).
[39] I. Yeh, L. Perera, and M. L. Berkowitz, Chem. Phys. Lett. **264**, 31 (1997).
[40] M. Roeselova, G. Jacoby, U. Kaldor, and P. Jungwirth, Chem. Phys. Lett. **293**, 309 (1998).
[41] D. Majumdar, J. Kim, and K. S. Kim, J. Chem. Phys. **112**, 101 (2000).
[42] Y. Gaudel, H. Gelabert, and M. Ashokkumar, Chem. Phys. **197**, 167 (1995).
[43] F. H. Long, X. Shi, H. Lu, and K. B. Eisenthal, Chem. Phys. Lett. **169**, 165 (1990).
[44] F. H. Long, X. Shi, H. Lu, and K. B. Eisenthal, J. Phys. Chem. **98**, 7252 (1994).
[45] J. A. Kloepfer, V. H. Vilchiz, V. A. Lenchekov, and S. E. Bradforth, J. Chem. Phys. **113**, 6288 (2000).
[46] V. H. Vilchiz, J. A. Kloepfer, A. C. Germaine, V. A. Lenchenkov, and S. E. Bradforth, J. Phys. Chem. A **105**, 1711 (2001).
[47] W. Sheu and P. J. Rossky, Chem. Phys. Lett. **202**, 186 (1993).
[48] W. Sheu and P. J. Rossky, Chem. Phys. Lett. **213**, 233 (1993).
[49] W. Sheu and P. J. Rossky, J. Phys. Chem. **100**, 1295 (1996).
[50] I. Bonhoure, A. M. Scheidegger, E. Wieland, and R. Daehn, Radiochim. Acta (unpublished).
[51] A. H. Narten, J. Phys. Chem. **74**, 765 (1970); T. Radnai, G. Pálinkás, G. I. Sász, and K. Z. Heinzinger, Z. Naturforsch. A **36**, 1076 (1981); A. H. Narten and R. L. Hahn, J. Phys. Chem. **87**, 3193 (1983).
[52] H. Ohtaki and T. Radnal, Chem. Rev. **93**, 1157 (1993).
[53] P. D'Angelo, A. Di Nola, A. Filipponi, N. V. Pavel, and D. Roccatano, J. Chem. Phys. **100**, 985 (1994).
[54] P. D'Angelo, A. Di Nola, M. Mangoni, and N. V. Pavel, J. Chem. Phys. **104**, 1779 (1996).

[55] C. Bressler, M. Saes, M. Chergui, D. Grolimund, and R. Abela, to appear in *Femtochemistry and Femtobiology*, edited by A. Douhal (World Scientific, Singapore, 2002).
[56] C. Bressler, M. Chergui, P. Pattison, M. Wulff, A. Filipponi, and R. Abela, Proc. SPIE **3451**, 108 (1998).
[57] A. Filipponi, unpublished data; see also U. Buontempo, A. Di Cicco, A. Filipponi, M. Nardone, and P. Postorino, J. Chem. Phys. **107**, 5720 (1997).
[58] M. Roeselova, U. Kaldor, and P. Jungwirth, J. Phys. Chem. A **104**, 6523 (2000).
[59] G. N. George and I. J. Pickering, *EXAFSPAK: A Suite of Computer Programs for the Analysis of X-ray Absorption Spectra*, Technical Report, Stanford Synchrotron Radiation Laboratory, Stanford, CA (1995).
[60] A. L. Ankudinov, B. Ravel, J. J. Rehr, and C. S. Conradson, Phys. Rev. B **58**, 7565 (1998).
[61] A. Reuther, A. Lauberau, and D. N. Nikogosyan, J. Phys. Chem. **100**, 16794 (1996); R. A. Crowell and D. M. Bartels, *ibid.* **100**, 17940 (1996).
[62] See also Ref. 55. We have measured the pulse height distribution of single x-ray pulses at beamline 5.3.1 for various energies in the 4–7 keV range. The statistical analysis yields an effective flux around 2×10^4 photons per pulse, while the calculated value is ca. 3×10^4 (P. Heimann, private communication). We have therefore utilized 10^4 photons per pulse as a reasonable value.
[63] R. W. Schoenlein, private communication.
[64] B. H. Wilk, Nucl. Instrum. Methods Phys. Res. A **398**, 1 (1997).